Electronic Supplementary Information (ESI)

A General Electrochemical Strategy for Upcycling Polyester Plastics into Added-value Chemicals by a $CuCo_2O_4$ Catalyst

1. Experimental Section

1.1 Chemicals

Cobaltous nitrate hexahydrate ($Co(NO_3)_2·6H_2O$), copper nitrate trihydrate ($Cu(NO_3)_2·3H_2O$) were obtained from Bailingwei Technology Co., Ltd. Ammonium fluoride (NH_4F) and urea were purchased from Sinopharm Chemical Reagent Co., Ltd. (Shanghai, China). Ni foam (thickness: 1.6 mm; porosity: ~98%) was purchased from Guangshengjia New Material Co., Ltd. All chemicals were analytical grade and used without further purification except for red phosphorus.

1.2 Pretreatment of plastics

5 g of plastics were soaked in 50 mL 5 M KOH aqueous solution for 12 h at 80°C with continuous stirring.

1.3 Synthesis of $CuCo_2O_4$ NWA/NF

The $CuCo_2O_4$ NWA/NF electrocatalyst was synthesized by a facile two-step procedure (Figure 1a). In a typical synthesis, the CuCo precursor nanowire arrays (CuCo-Pre NWA/NF) were directly grown on a Ni foam through a straightforward hydrothermal process. Firstly, 1 mmol of $Co(NO_3)_2·6H_2O$, 0.5 mmol of $Cu(NO_3)_2·3H_2O$ were dissolved into 40 mL of deionized (DI) water, followed by the addition of 3 mmol of NH_4F and 6 mmol of urea into the solution. After stirring continuously at room temperature for 10 min, the solution was then transferred to a 50 mL Teflonlined stainless steel autoclave. A piece of Ni foam (2.5 cm × 4 cm) was washed with a 3 M HCl solution and DI water for 20 min to get rid of the possible surface oxide layer, and the conductive substrate was then immersed in the solution. Afterward, the autoclave was sealed and maintained at 120 °C for 6 h. After cooling to room temperature naturally, the substrate was then taken out and cleaned by DI water and ethanol several times before being fully dried at 60 °C overnight under vacuum. Similarly, the pure Co precursors or Cu precursors were prepared by the similar procedure with the only addition of 1.5 mmol of $Co(NO_3)_2·6H_2O$ or $Cu(NO_3)_2·3H_2O$,respectively. For the synthesis of $CuCo_2O_4$ NWA/NF, a piece of CuCo-Pre NWA/NF (2 cm x 1 cm) was placed in the central region of a tubular furnace. Finally, it was calcined at 300 °C for 3 h under an air atmosphere with a heating rate of 2 °C min^{-1}.

1.4 Structural Characterization

The powder X-ray diffraction pattern was collected a 18KW/D/max2550VB/PC (40 KV, 200 mA) equipped with Cu Kα radiation under a scan rate of 2 degree/min. ^{1}H and ^{13}C nuclear magnetic resonance (NMR) spectroscopy was recorded on a 600 MHz/AVANCE 400 (Bruker). Scanning electron microscopy (SEM) was conducted on a Hitachi S-4800 field emission scanning electron microscope. Transmission electron microscopy (TEM) and high-resolution TEM (HRTEM) were conducted on a JEOL-2100F (Japan) microscope operating at a voltage of 200 kV. Raman measurements were recorded using a Renishaw inVia-Reflex spectrometer with a 532 nm excitation laser. XPS spectra were firstly deoxygenated under Ar for 1 h and then investigated on a Thermo Scientific ESCALAB 250XI spectroscopy equipped with an Al Kα X-ray source and the spectra were calibrated with a binding energy of 284.6 eV for C 1s.

1.5 Electrochemical measurements

All electrochemical experiments were performed in an H-type cell (100 mL) separated by proton exchange membrane (Nafion 117) on CHI660e electrochemical workstation (Chenhua Instrument Inc., shanghai, China). The tests were carried out in a standard three-electrode system with a working electrode, a platinum sheet (1 cm^2) as the counter electrode, and an Hg/HgO reference electrode at room temperature. The as-synthesized catalysts on NF electrodes ($CuCo_2O_4$ NWA/NF) were used directly as working electrodes (geometric electrode area of 1 cm^2, mass loading of ~1.2 g cm^{-2}). The electrolyte solution is 1M KOH with or without 25mg/mL PET hydrolysate. All curves were measured at a scan rate of 5 mV s^{-1} without iR-compensation unless specified. All potentials in this study were converted to RHE reference scale based on the Nernst equation listed as follows: $E_{RHE} = E_{Hg/HgO} + 0.098 + 0.059$ pH. EIS measurements were performed in a frequency range from 10^5 to 0.01 Hz with a perturbation of 5 mV. The electrochemical double layer capacitances (Cdl) of various samples were confirmed by CV in the potential region without faradaic process to calculate the ECSA.

To demonstrate the practicality of our catalytic system, a two-electrode membrane-electrode assembly (MEA) electrolyzer flow reactor was constructed using $CuCo_2O_4$ NWA/NF as anode (geometric electrode area of 2 cm × 2 cm, mass loading of ~1.2 g cm^{-2}) and Pt/NF as cathode (geometric electrode area of 2 cm × 2 cm, mass

loading of ~1g cm^{-2}) for electro-reforming real-world PET plastic bottles. The measurements were performed at room temperature, in which 5.0 M KOH aqueous solution and 5 M KOH/ 200 mg L^{-1} PET hydrolysate were added into the cathode side and anode side with a flow rate of 0.1 mL min^{-1} by a silicone tube and a peristaltic pump. The configuration of MEA electrolyzer flow reactor composed of polytetrafluoroethylene (PEFT) flow plate, rubber gasket, proton exchange membrane and as-prepared electrocatalysts.

1.6 Product Analysis

The liquid products can be analyzed by nuclear magnetic resonance (NMR) spectrometer. ^{1}H and ^{13}C NMR spectra were recorded on a 600 MHz/AVANCE 400 (Bruker), In which 300 μL electrolyte was added with 300 μL D_2O and 30 μL dimethyl sulfoxide（DMSO）used as an internal standard. Meanwhile, the gas products (CO_2 and CO produced at anode, H_2 produced at cathode) can be measured by a gas chromatograph ((GC-2014C, 5 Å molecular sieve column, 3 m × 2 mm, DINJ 50 °C, DTCD 100 °C, column temperature 50 °C, carrier gas flow 30 mL min^{-1}), quantified by the external standard method.

The yield (%) and selectivity (%) of formate formation can be determined by the following Eq. (1) and (2), respectively.

$$\text{Yeild}(\%) = \frac{N(\text{formate yield})}{2N(\text{initial EG})} \times 100\% \quad \text{..... Eq. (1)}$$

$$\text{Selectivity}(\%) = \frac{N(\text{formate yield})}{2N(\text{consumed EG})} \times 100\% \quad \text{..... .....Eq. (2)}$$

The Faraday efficiency (%) of the product formation can be determined by the following Eq. (3):

$$\text{FE}(\%) = \frac{N(\text{formate yield})}{\text{toal charge passed}/3 \times 96485} \times 100\% \quad \text{..... Eq. (3)}$$

1.7 Computational methods:

Spin-polarized density functional theory (DFT) calculations were performed to optimize the cell shape and the atomic positions of the $CuCo_2O_4$, Co_3O_4, and CuO structures by Vienna *ab initio* simulation package (VASP)[1] using the projector augmented wave (PAW) potentials with a planewave cutoff energy of 450 eV.[2, 3]The

generalized gradient approximation (GGA) functional of Perdew, Burke, and Ernzerhof (PBE) was applied as the exchange-correlation functional.[4] To better describe the localized d-electrons of Co in $CuCo_2O_4$ and Co_3O_4 structures, the DFT+U approach was utilized with $U_{Co} = 3.0$.[5] The convergence criteria of electronic energies and atomic forces for all calculations were 10^{-5} eV and 0.03 eV/Å. The optimized cell parameters were found to be: a = b = c = 8.07 Å, α = β = γ = 90° for $CuCo_2O_4$, a = b = c = 8.35 Å, α = β = γ = 90° for Co_3O_4, and a = b = c = 4.20 Å, α = β = γ = 90° for CuO.

In order to compute the adsorption energies at the surface of different catalysts, the (220) slab of $CuCo_2O_4$ and Co_3O_4, and the (200) slab of CuO were constructed within four metal layers based on the experimental results. A vacuum region of 15 Å was added to the surface to eliminate the effects between two adjacent layers. During the calculation, the bottom two metal layers were fixed at their bulk positions using a $3 \times 3 \times 1$ Gamma k-point grid. The calculated binding energy (E_{ads}) was evaluated based on the following equation:

$$\Delta E_{ads} = E_{sur+adsorbate} - E_{sur} - E_{adsorbate}$$

where $E_{sur+adsorbate}$, E_{sur}, and $E_{adsorbate}$ are the obtained energies for the slab system containing the adsorbate, the energy of the slab, and the energy of the adsorbate in a vacuum, respectively. Here, 'adsorbate' refers to chemisorbed ethylene glycol, OH, or H_2O species.

1.8 techno-economic analysis:

Costs:

1. Material costs

Material costs: 1 ton PET (500 $/t), 1.4 ton KOH (850 $/t), 5 ton water and 1.2 ton H_2SO_4 (148 $/t).

$$Material\ \cos t = 1874\,\$$$

2. Electricity costs:

The total charge required for electro-reforming per ton of PET can be calculated as follows:

$$Q = \frac{n \times F \times N}{FE} = \frac{10\text{^}6 \times 2 \times 96485 \times 3}{0.8} = 3.77 \times 10\text{^}9C$$

Where Q is the total charge, n is the mole of EG (1 ton of PET), F is the Faraday's constant (96485) and N is the number of electron transfer (3), FE is the faradaic efficiency of formate production from PET electro-reforming.

The power required to maintain electrolysis process can be calculated as follows,

assuming that the cell potential is 1.5 V:

$$P = \frac{U \times Q}{3600 \times f} = \frac{1.5 \times 3.77 \times 10\text{^}9}{3600 \times 0.8} = 1964\,(\text{kWh})$$

Where U is the cell potential, f is the capacity factor (0.8).

$$\text{Electricity cost} = P \times \text{Price} = 1964 \times 0.118\ \$ = 232\ \$$$

3. Separation costs:

The separation costs are 50 % of electricity costs. Therefore:

$$\text{Separation cost} = 232 \times 0.5 = 116\ \$$$

4. Miscellaneous costs:

In the electro-reforming PET process, miscellaneous costs including capital costs, maintenance costs and operating costs are about 765 $.

$$\text{Miscellaneous cost} = 765\ \$$$

5. Total plant gate levelized cost:

Finally, the total cost can now be calculated by adding up all 4 components:

$$\text{Toal cost} = 1874\ \$ + 232\ \$ + 116\ \$ + 765\ \$ = 2987\ \$$$

Product value:

After electrolysis, 1 ton of PET feedstock finally gave 0.456 ton HCOOH (1479.7 $/t), 0.842 ton PTA (961.8 $/t), 2.134 ton K_2SO_4 (887.8 $/t) and 0.0309 ton H_2 (7210 $/t).

$$\text{Product value} = 3601\ \$$$

Potential profit:

Therefore, the total income of electrolysis per ton of PET can be calculated as follows:

$$\text{Toal profit} = \text{Product value} - \text{toal cost} = 3601\text{-}2987 = 614\ \$$$

2 Results and Discussion

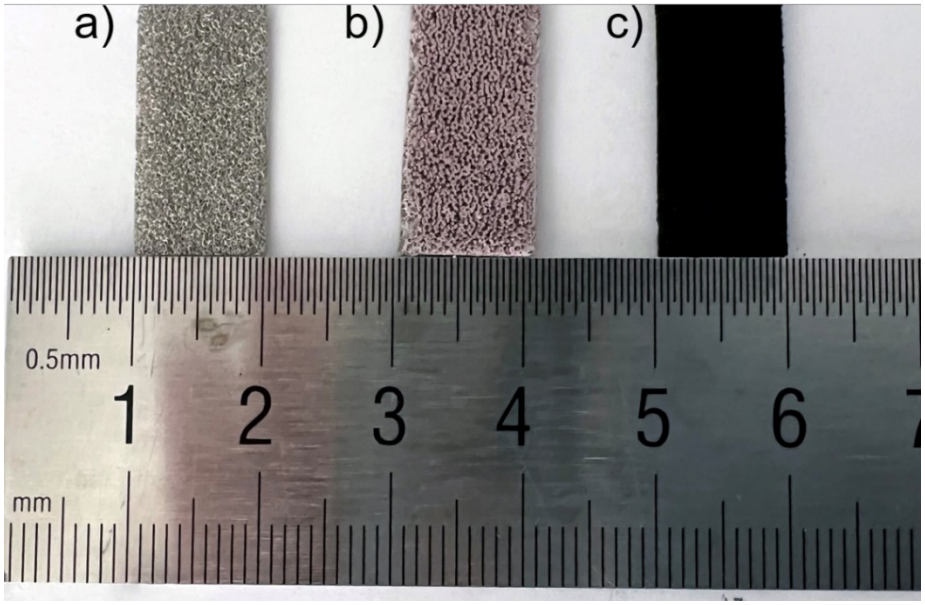

Fig. S1. Digital images of a) NF; b) CuCo-Pre NWA/NF; c) $CuCo_2O_4$ NWA/NF.

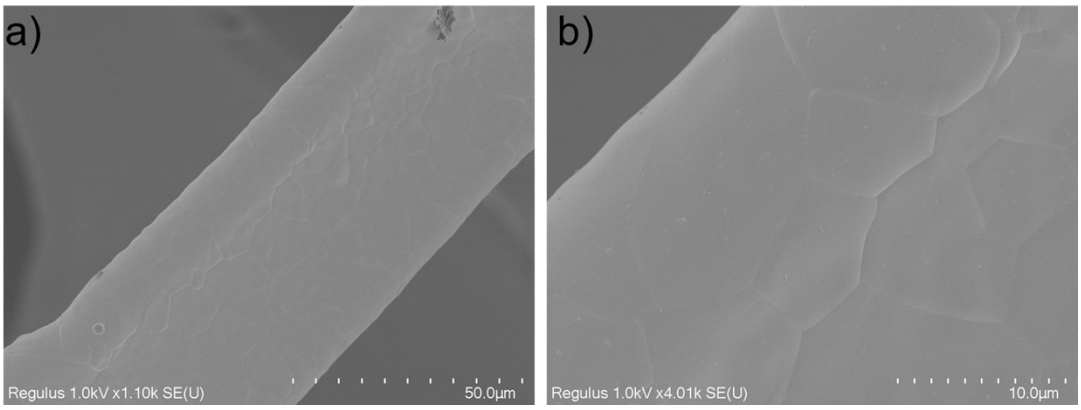

Fig. S2. SEM images of NF with different magnifications.

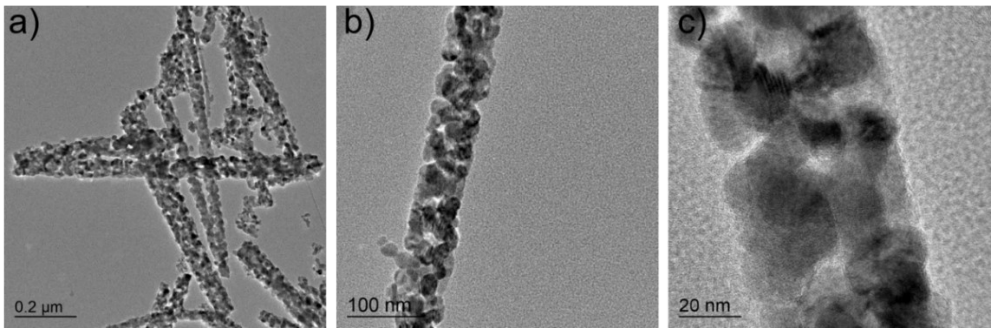

Fig. S3. TEM images of $CuCo_2O_4$ NWA/NF with different magnifications.

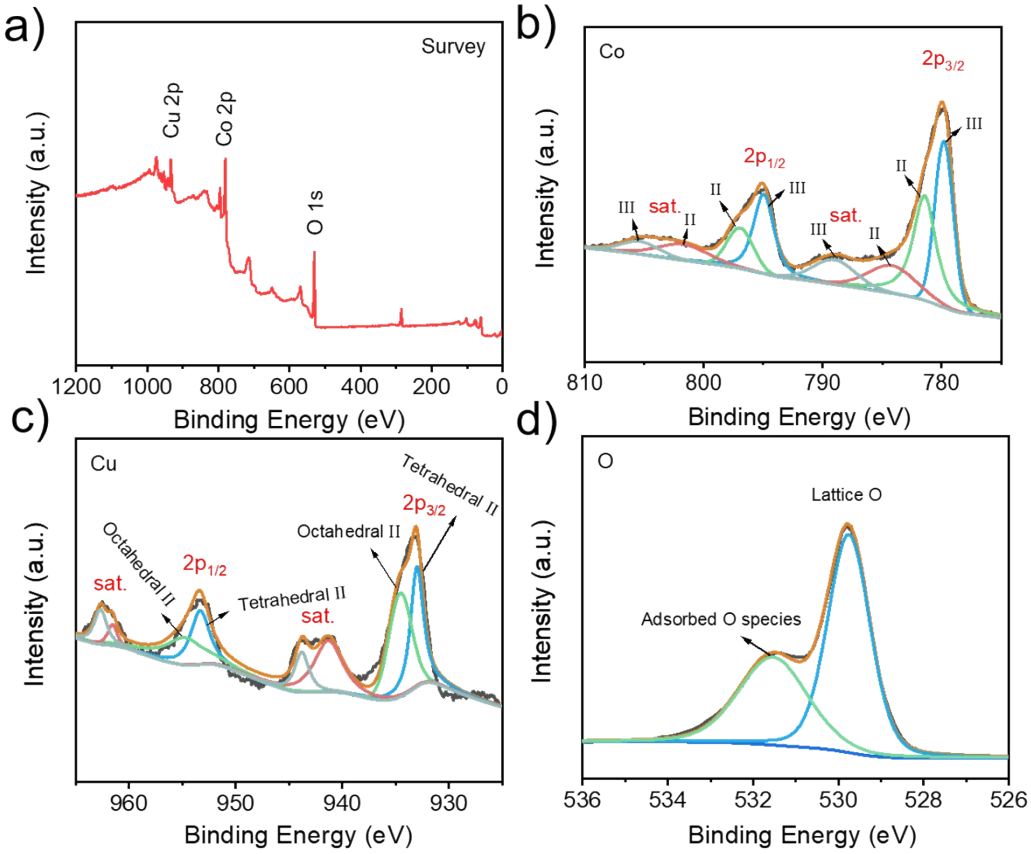

Fig. S4. XPS spectra of the as-prepared $CuCo_2O_4$ NWA: a) survey spectrum, b-d) corresponding high resolution XPS spectra of Cu 2p, Co 2p and O 1s.

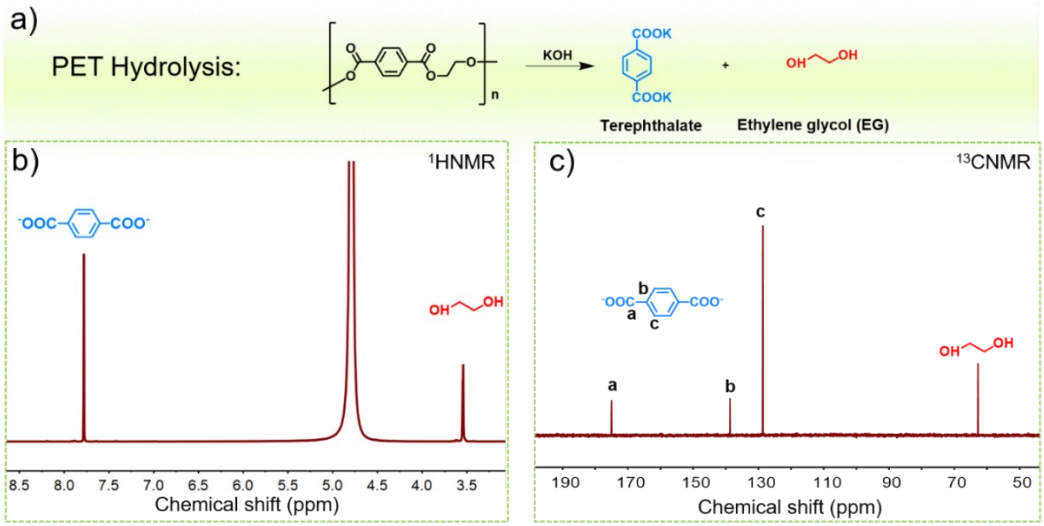

Fig. S5. a) PET hydrolysis formula; b) ^{1}H NMR and c) ^{13}C NMR measurements of PET hydrolysate.

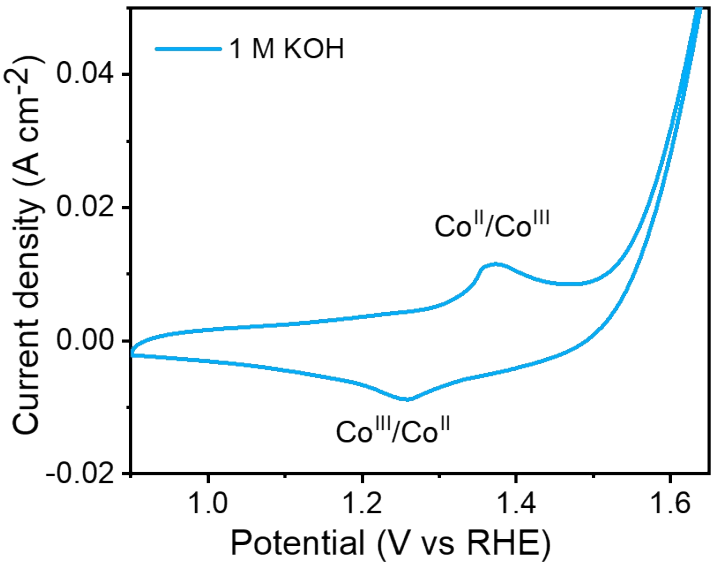

Fig. S6. Cyclic voltammetric (CV) curves of $CuCo_2O_4$ NWA/NF in 1 M KOH at a scan rate of 5 mV s^{-1}.

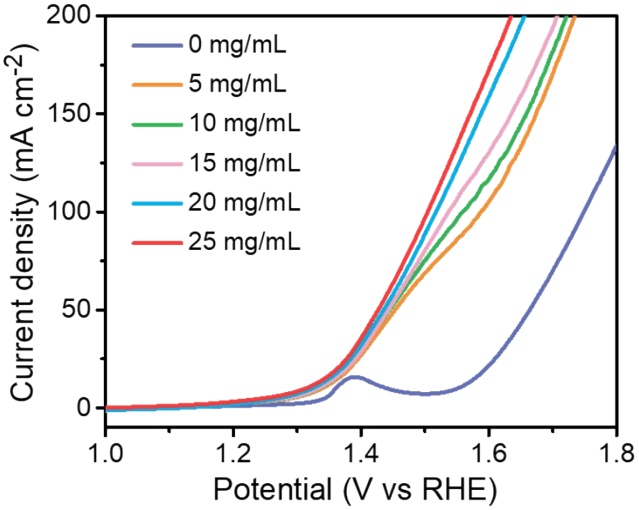

Fig. S7. LSV curves of $CuCo_2O_4$ NWA/NF in 1 M KOH with different concentrations of PET.

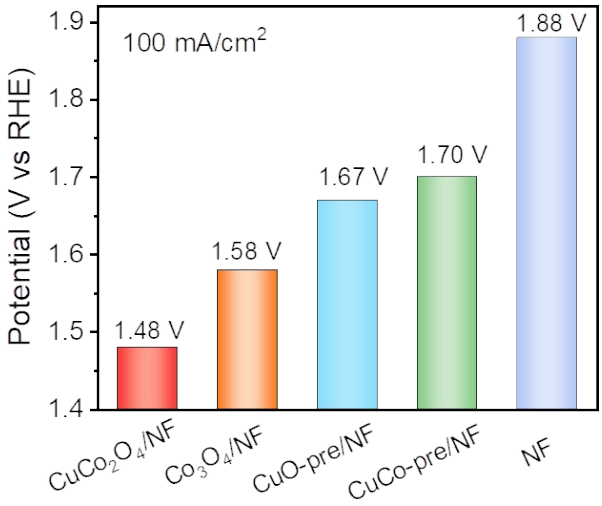

Fig. S8. Comparisons of the anodic potentials at a current density of 100 mA cm^{-2} for $CuCo_2O_4$ NWA/NF in 1 M KOH with PET hydrolysate.

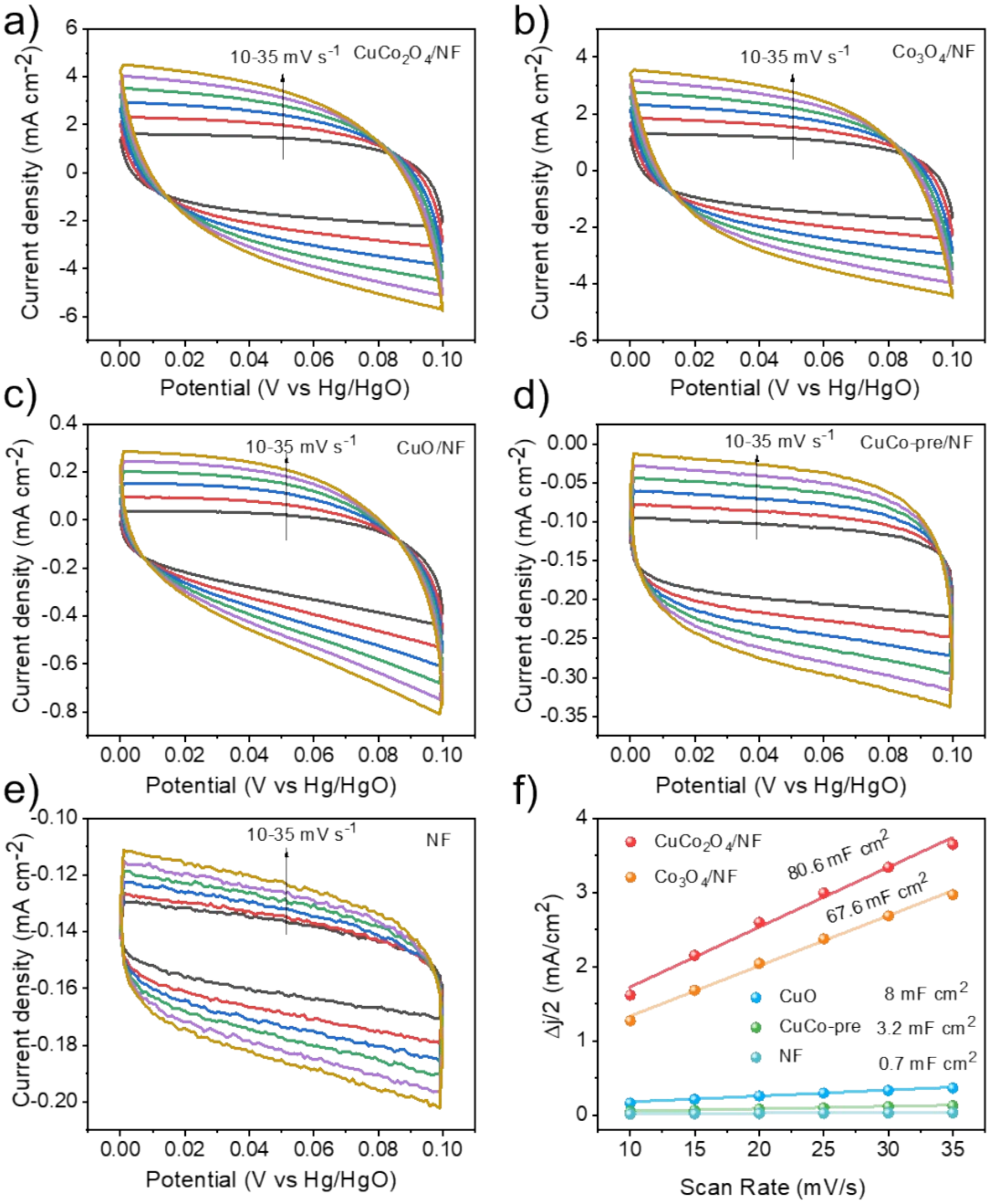

Fig. S9. The CV curves of a) $CuCo_2O_4$ NWA/NF; b) Co_3O_4/NF; c)CuO/NF; d) CuCo-Pre NWA/NF; e) bare NF; f) C_{dl} values at potential of 0.05 V (vs. Hg/HgO).

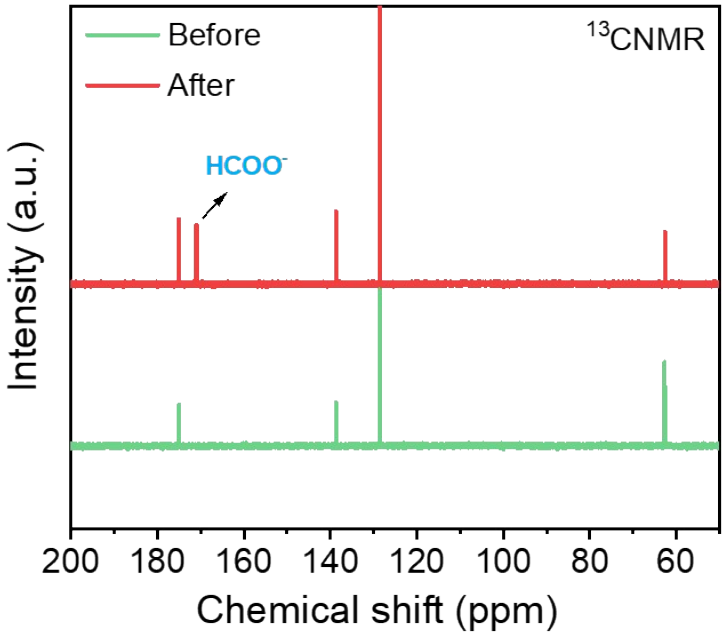

Fig. S10. ^{13}C NMR spectra of products before and after electro-reforming on $CuCo_2O_4$ NWA/NF electrode.

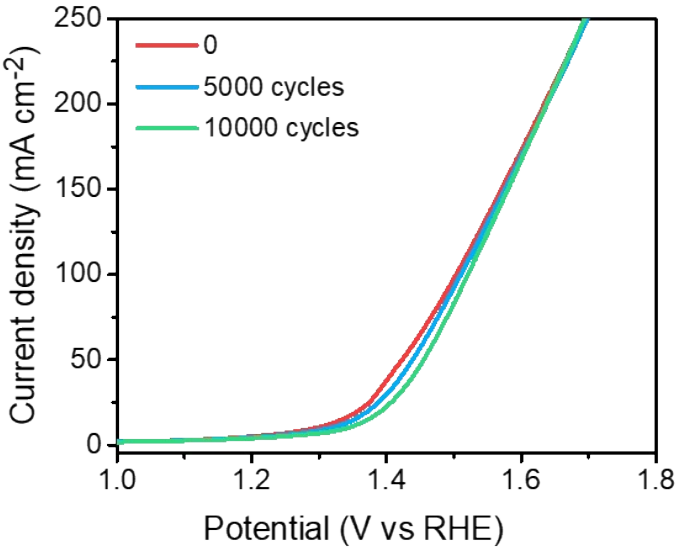

Fig. S11. LSV curves for $CuCo_2O_4$ NWA/NF electrode in 1.0 M KOH with and without TPA addition.

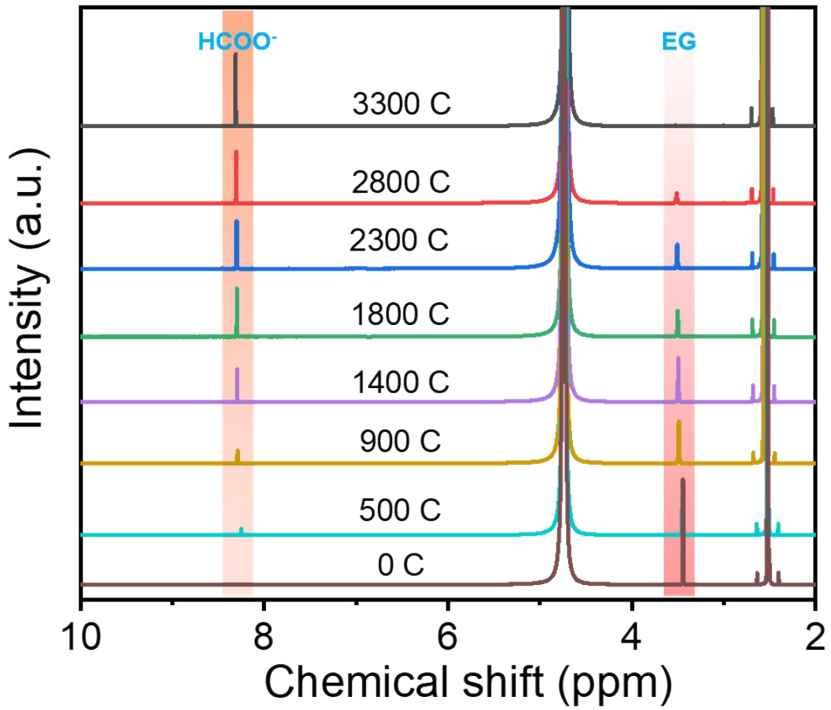

Fig. S12. a) ^{1}H NMR measurements of EG oxidation.

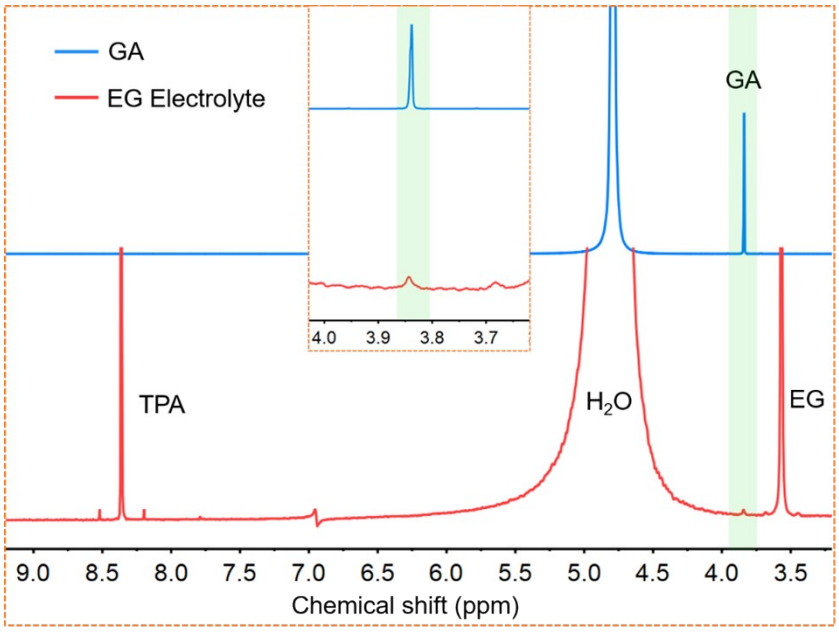

Fig. S13. ^{1}H NMR of GA and EG electrolyte.

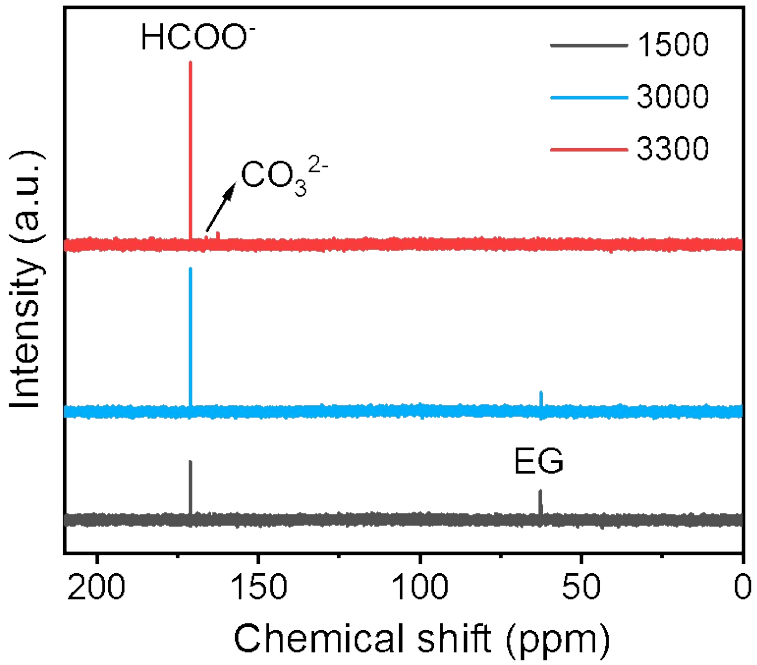

Fig. S14. a) ^{13}C NMR measurements of EG oxidation.

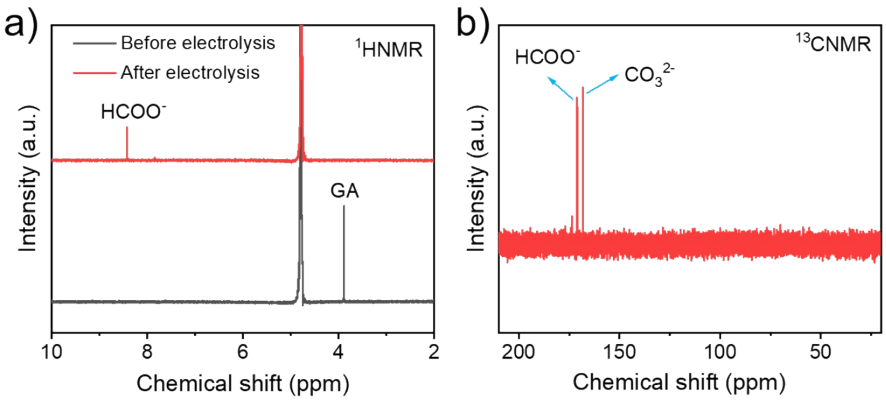

Fig. S15. a) ^{1}H NMR and b) ^{13}C NMR measurements of GA oxidation.

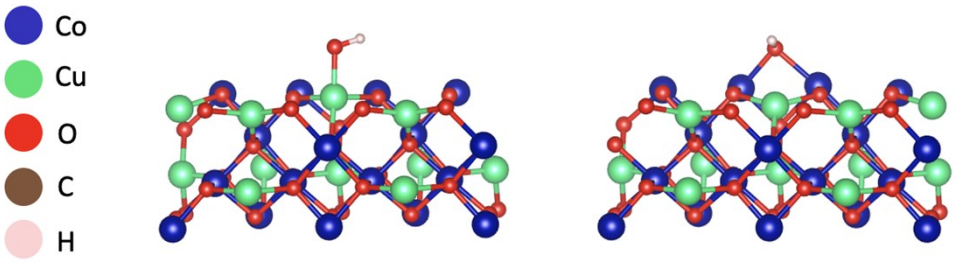

Fig. S16. Optimized configurations of OH* adsorbed on Cu atom (left) and Co atom (right) of $CuCo_2O_4$. The calculated energies for two structures are E_{DFT} = -319.15 eV (left) and E_{DFT} = -320.77 eV (right), respectively.

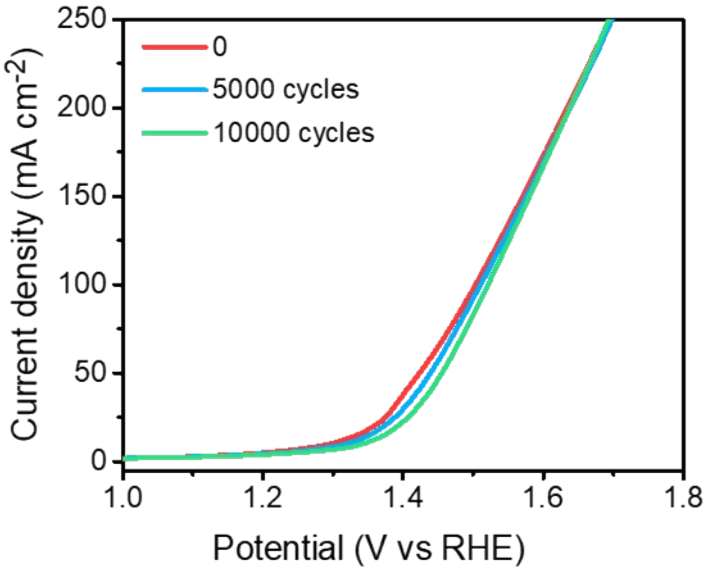

Fig. S17. LSV curves of $CuCo_2O_4$ NWA/NF after successive CV test.

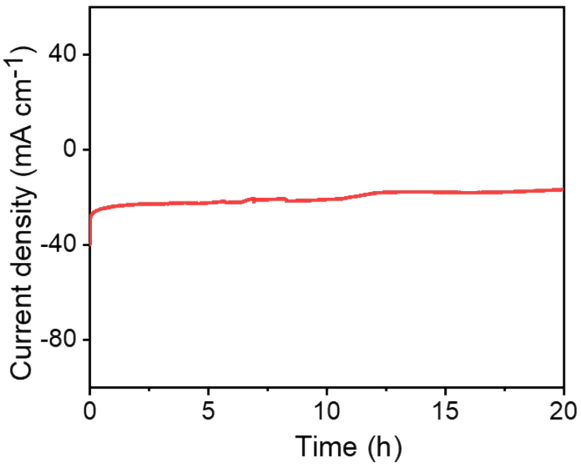

Fig. S18. The chronoamperometry curve of $CuCo_2O_4$ NWA/NF electrode recorded at potential of 1.35 V (vs. RHE) in 1.0 M KOH/PET hydrolysate.

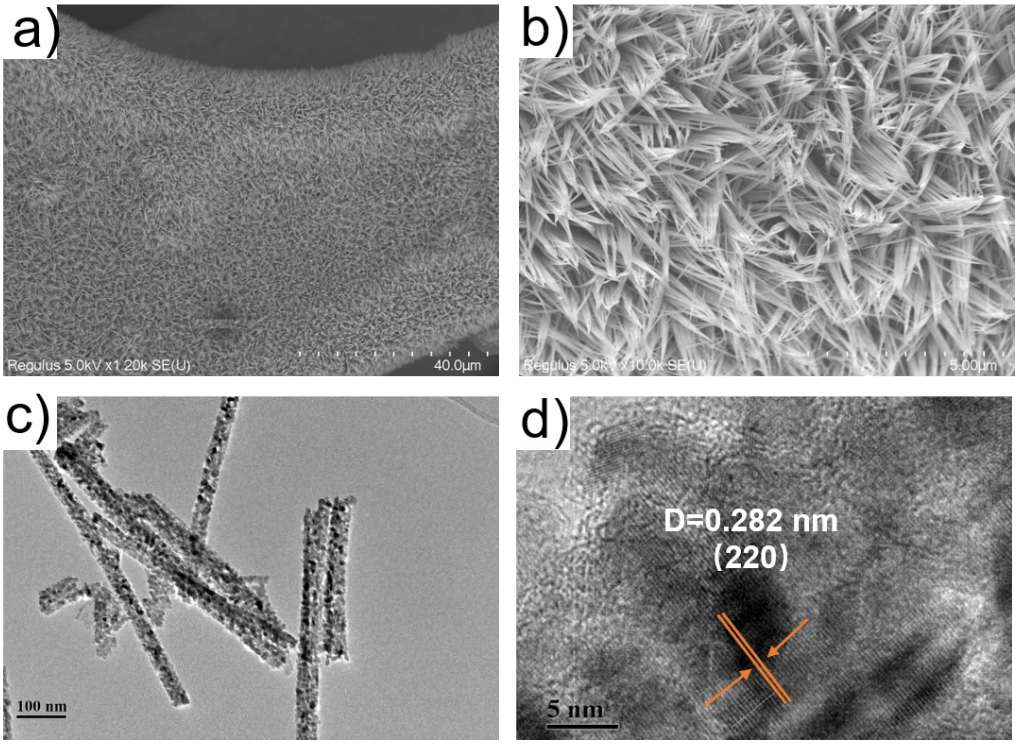

Fig. S19. a-b) SEM images; c-d) TEM images of $CuCo_2O_4$ NWA after electrocatalytic reaction.

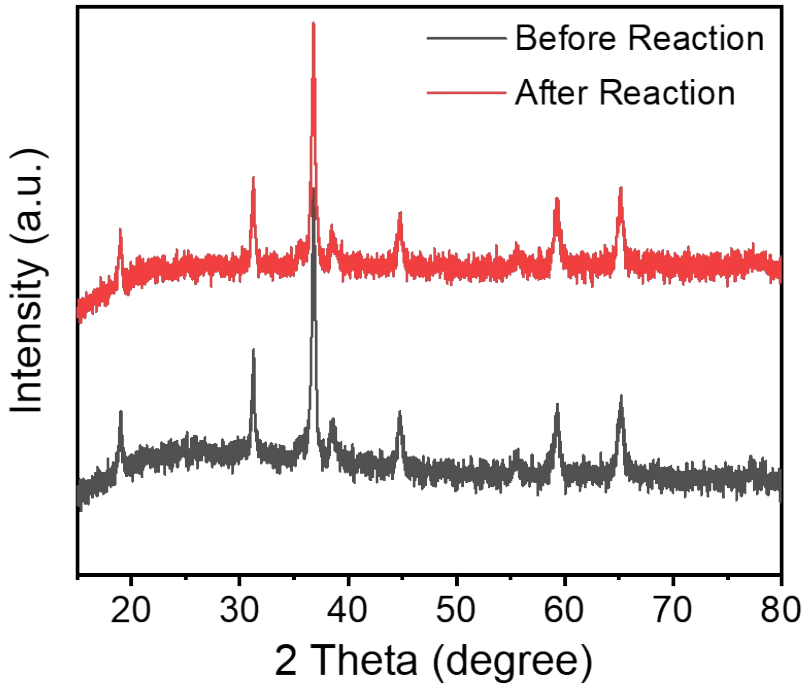

Fig. S20. XRD patterns of $CuCo_2O_4$ NWA/NF electrode before and after electrolysis.

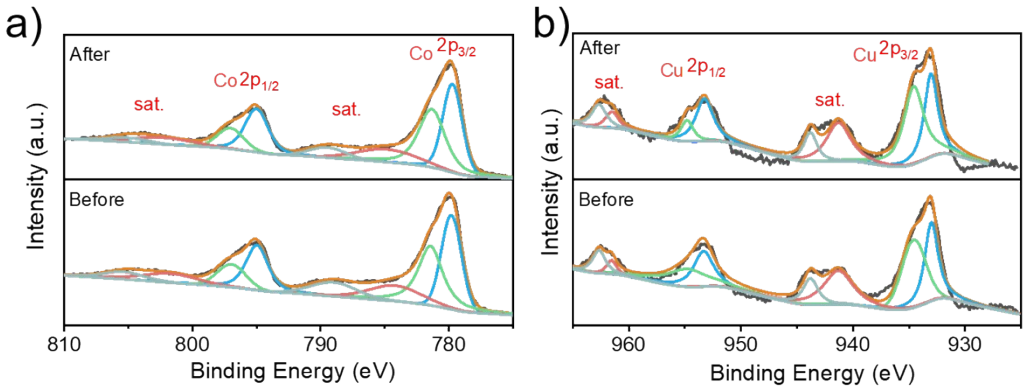

Fig. S21. XPS spectra of $CuCo_2O_4$ NWA/NF electrode before and after electrolysis.

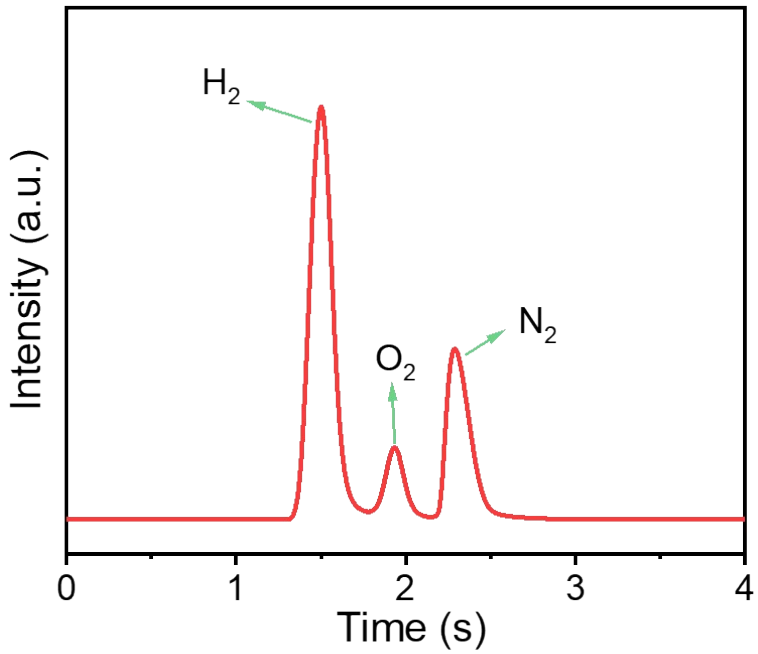

Fig. S22. GC spectra of the gas produced after electrocatalytic reaction reaction at the cathode.

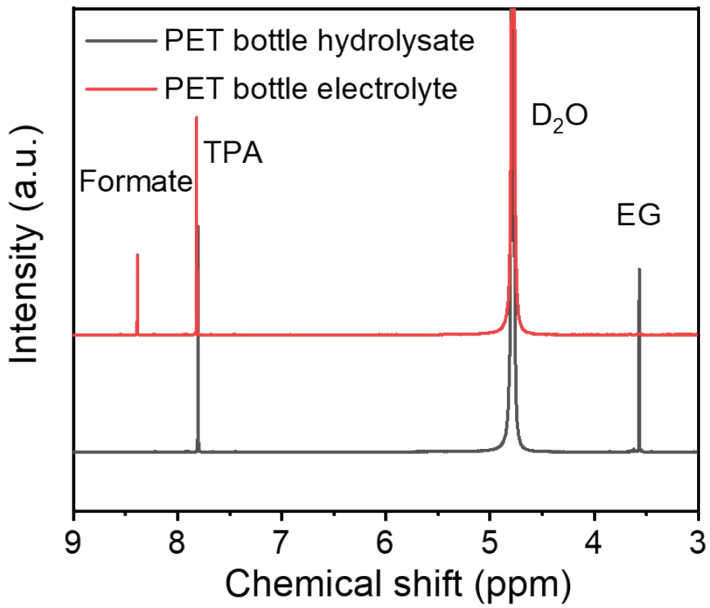

Fig. S23. ^{1}H NMR spectra of products before and after electro-reforming real-world PET bottles on $CuCo_2O_4$ NWA/NF electrode.

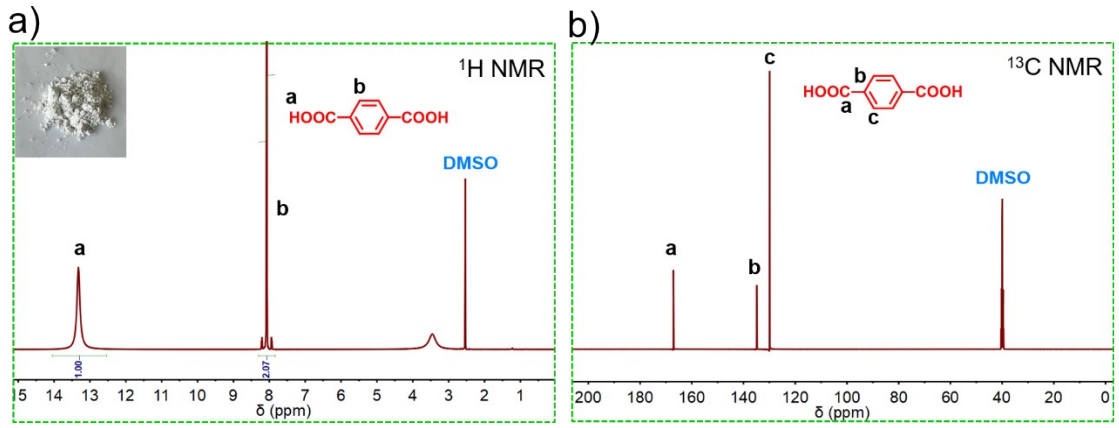

Fig. S24. a) ^{1}H NMR spectrum b) ^{13}C NMR spectrum of TPA (inset: digital photograph of TPA powder).

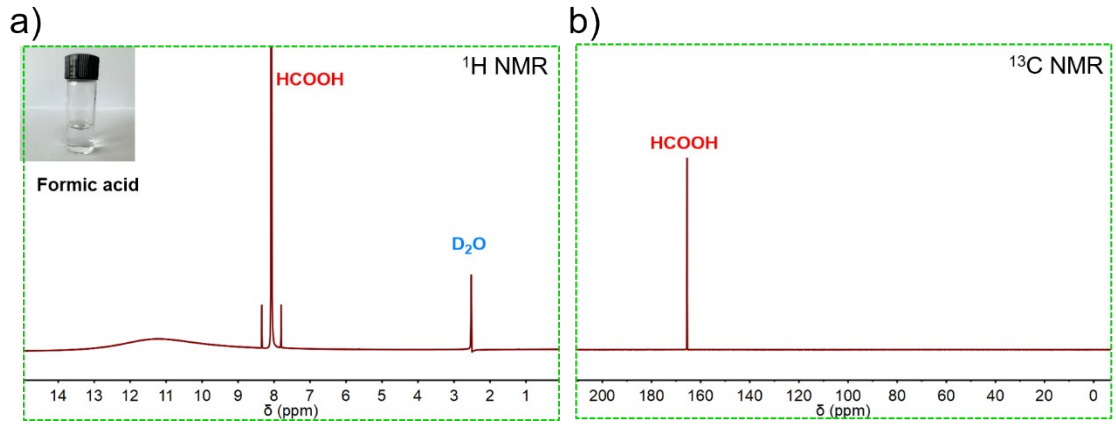

Fig. S25. a) ^{1}H NMR spectrum b) ^{13}C NMR spectrum of formic acid (inset: digital photograph of formic acid).

We subsequently carried out a preliminary techno-economic analysis to evaluate the economic feasibility of this electrocatalytic strategy using a modified model reported by Sargent group. It can be estimated that electro-reforming per ton of waste PET can get a net profit of ~614 $.

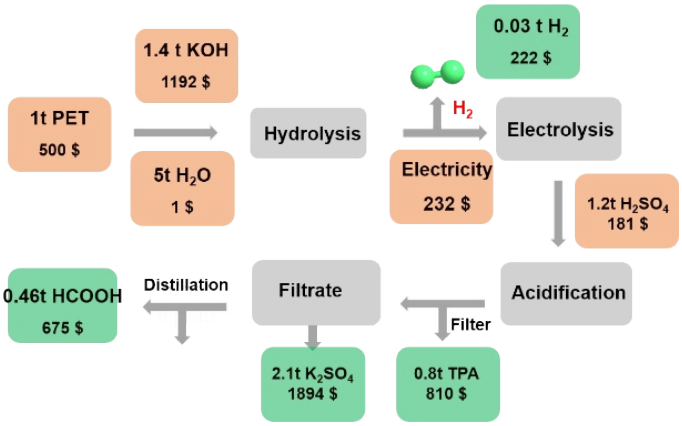

Fig. S26. Schematic illustration of the electro-reforming process, the final products are TPA, HCOOH, $K_2SO_4$and H_2.

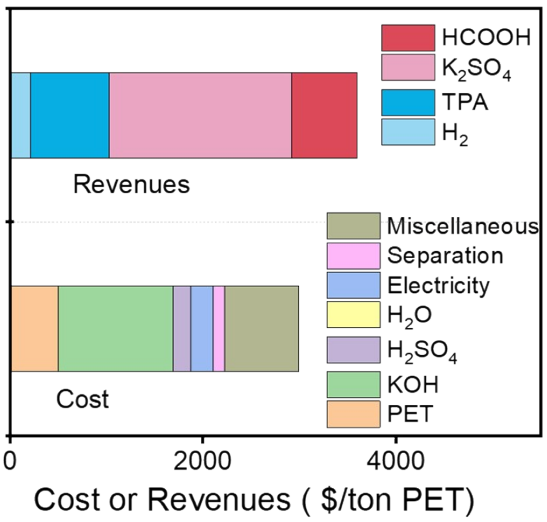

Fig. S27. Techno-economic analysis of this electro-reforming process. Assuming 97% of TPA, 95% of HCOOH, 98% of K_2SO_4 and 99% of H_2 are recycled.

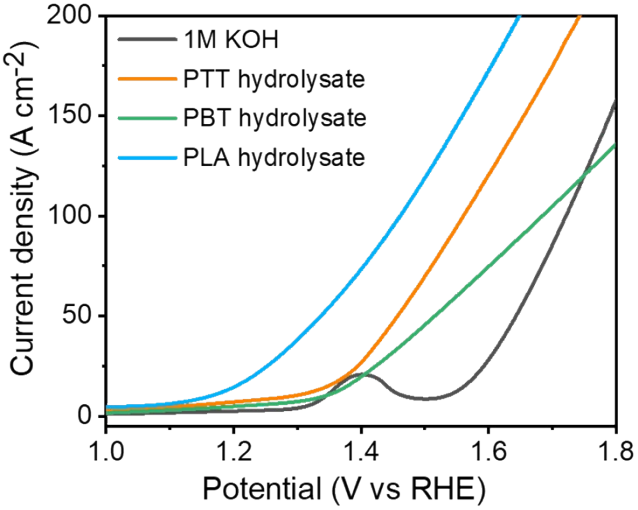

Fig. S28. LSV curves for $CuCo_2O_4$ NWA/NF electrode in different plastic hydrolysates.

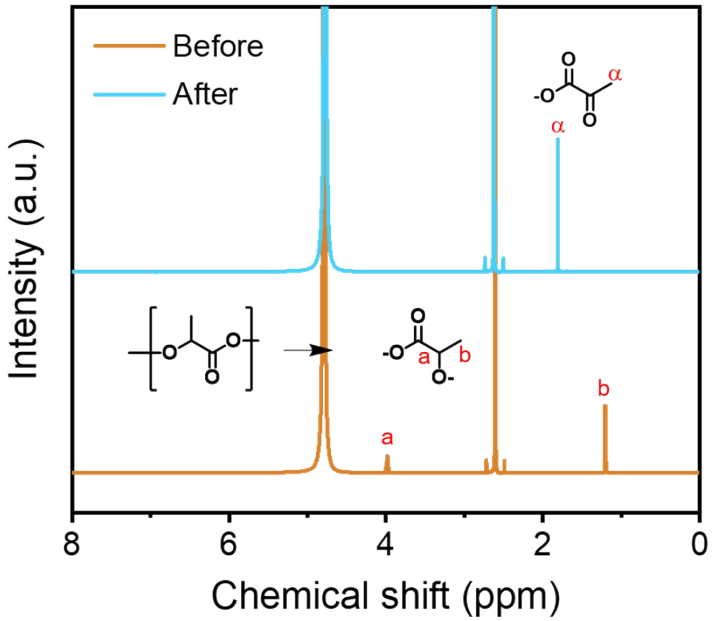

Fig. S29. ^{1}H NMR spectra of products before and after electro-reforming PLA on $CuCo_2O_4$ NWA/NF electrode.

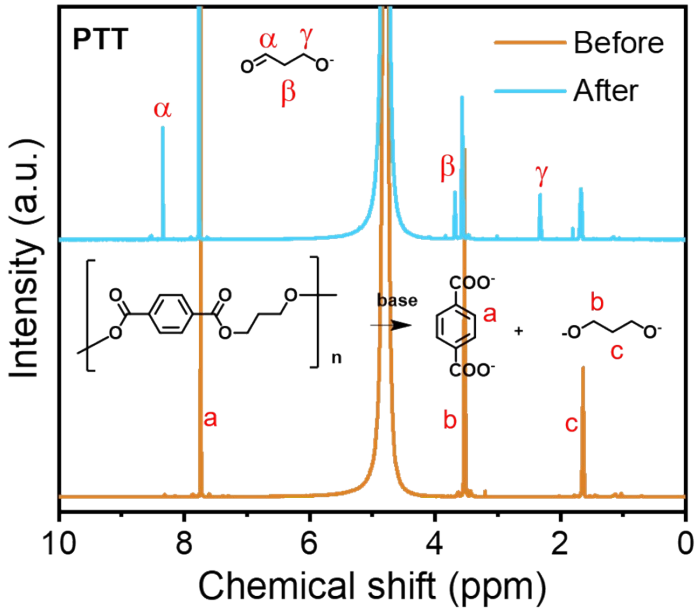

Fig. S30. ^{1}H NMR spectra of products before and after electro-reforming PTT on $CuCo_2O_4$ NWA/NF electrode.

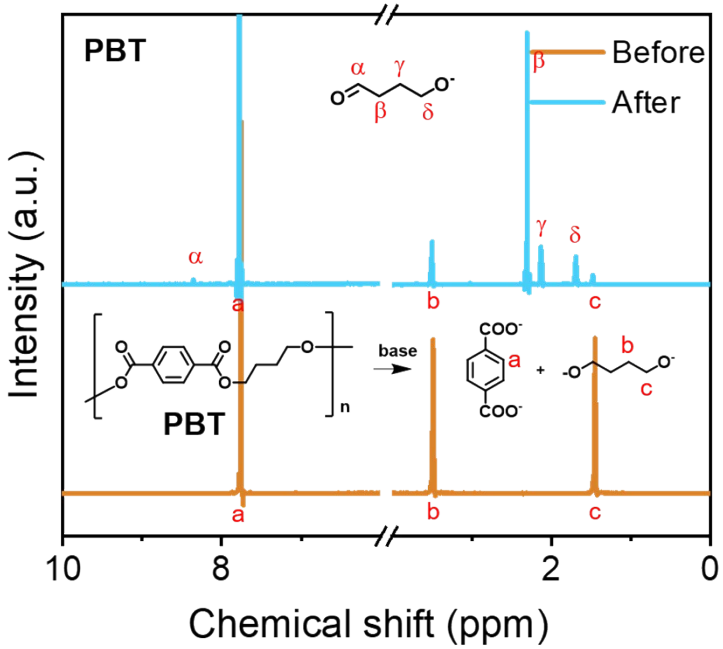

Fig. S31. ^{1}H NMR spectra of products before and after electro-reforming PBT on $CuCo_2O_4$ NWA/NF electrode.

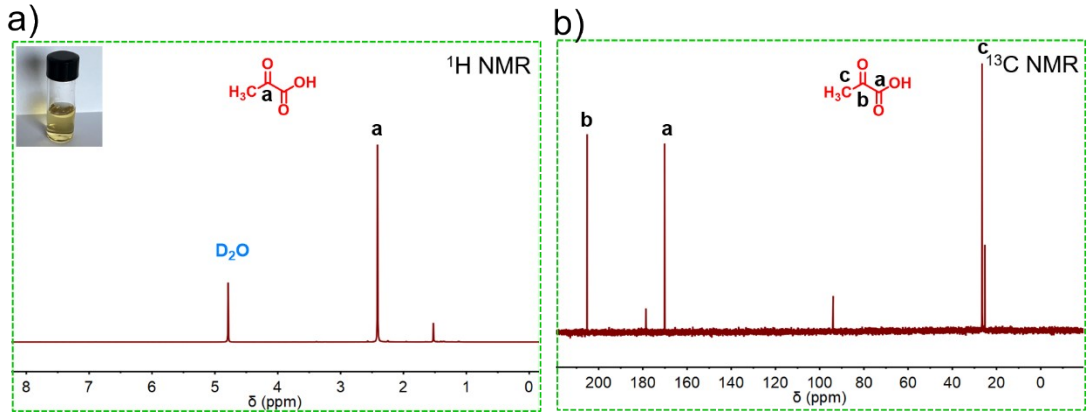

Fig. S32. a) ^{1}H NMR spectrum b) ^{13}C NMR spectrum of pyruvic acid (inset: digital photograph of pyruvic acid).

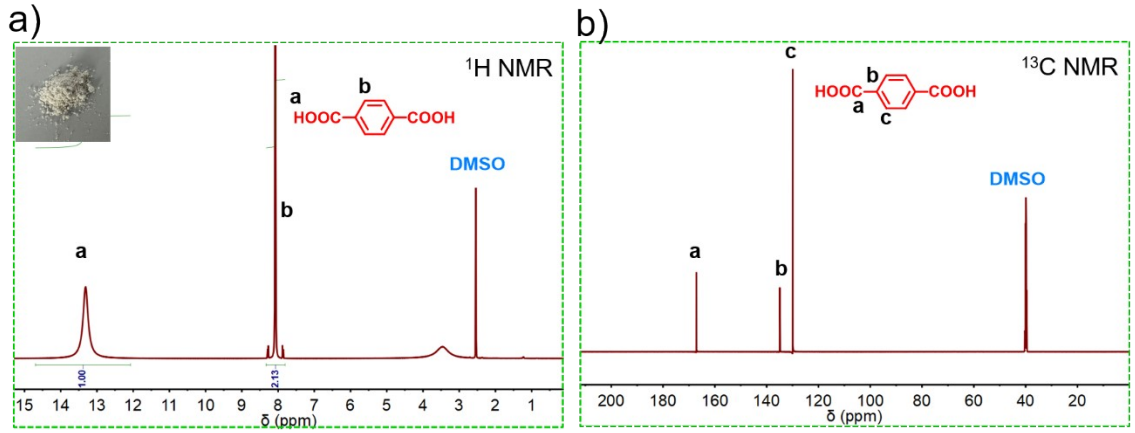

Fig. S33. a) ^{1}H NMR spectrum b) ^{13}C NMR spectrum of TPA (inset: digital photograph of TPA powder).

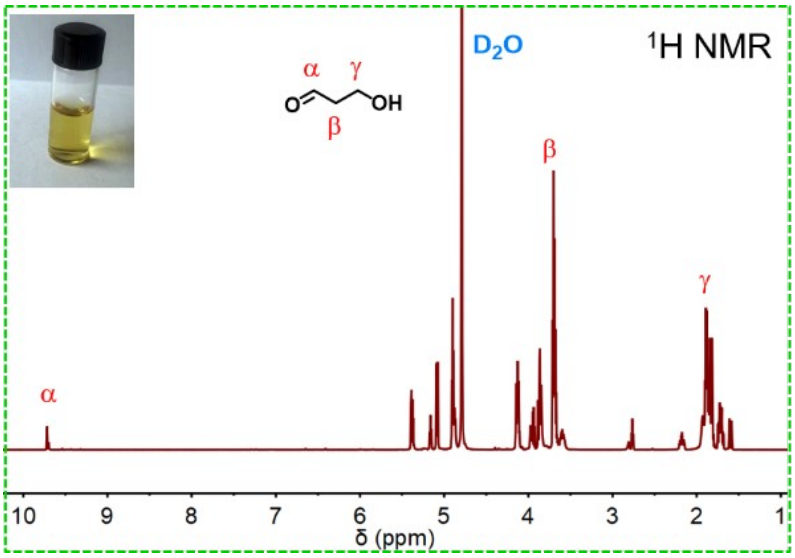

Fig. S34. a) [1]H NMR spectrum 3-hydroxypropionaldehyde (inset: digital photograph of 3-hydroxypropionaldehyde).

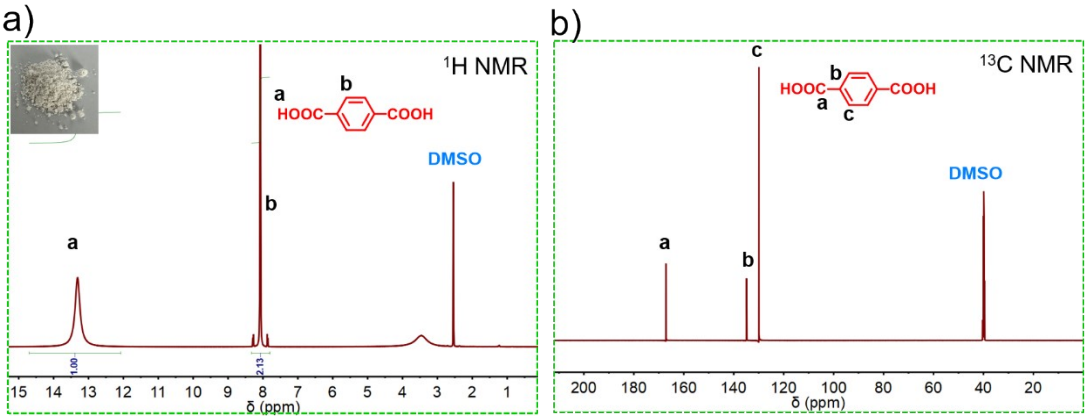

Fig. S35. a) 1H NMR spectrum b) 13C NMR spectrum of TPA (inset: digital photograph of TPA powder).

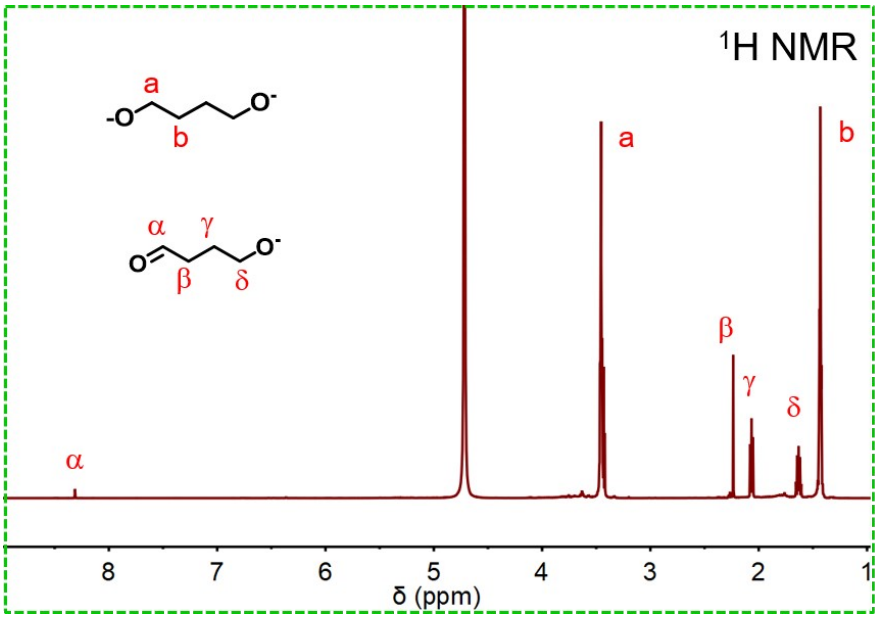

Fig. S36. a) [1]H NMR spectrum of butanediol and 4-hydroxybutyr-aldehyde in acidic aqueous solution.

Table S1. Comparison of state-of-the-art catalysts for alcohol oxidation in 1 M KOH.

Electrocatalysts	Anodic potential (V, 10mA cm^{-2})	Alcohols	Ref.
Co_2CuO_4 NWA/NF	1.23	EG	This work

Co@CoO-1/rGO	1.12 (20)	Glucose	*J. Mater. Chem. A* **2022** (Ref.6)
$CoNi_{0.25}P$/NF	1.7 (350)	EG	*Nat. Commun.* **2021** (Ref.7)
CuONS/CF	1.36 (100)	MeOH	*Angew. Chem. Int. Ed.* **2021** (Ref.8)
$Ni(OH)_2$/NF	1.36 (100)	MeOH	*Appl. Catal., B* **2020** (Ref.9)
Co_2CuO_4	1.3	Glycerol	*ACS Catal* **2020** (Ref.10)
NiFeOx-NF	1.3 (87.6)	Glucose	*Nat. Commun.* **2020** (Ref.11)
Ni_3C	1.55	MeOH	*Angew. Chem. Int. Ed.* **2020** (Ref.12)
$Co(OH)_2$@HOS/CP	1.47 (100)	MeOH	*Adv. Funct. Mater.***2020** (Ref.13)
Ni-Mo-N/CFC	1.30	Glycerol	*Nat. Commun.* **2019** (Ref.14)
CoCu-UMOF Ns	1.365	MeOH	*ACS Appl. Mater. Interfaces* **2018** (Ref.15)
NiFe LDH	1.32 (20)	HMF	*ACS Catal* **2018** (Ref.16)
Ni_2P/Ni/NF	1.43 (onset)	Furfural	*ChemNanoMat* **2017** (Ref.17)
Co_3O_4 NSs/CP	1.445	Ethanol	*ACS Cent. Sci.* **2016**

			(Ref.18)
Ni_3S_2/NF	1.35 (onset)	HMF	*J. Am. Chem.Soc.* **2016** (Ref.19)

All the potentials here are V vs. RHE. All the potentials correspond to 10 mA cm^{-2} unless otherwise marked.

Table S2. DFT calculated binding energy of EG, OH, and H_2O as well as energy difference between *EG and *OH on $CuCo_2O_4$, Co_3O_4, and CuO.

Surface	ΔE_{*EG}	ΔE_{*OH}	ΔE_{*H2O}	ΔE_{*EG} - ΔE_{*OH}
Co_2CuO_4	-0.75 eV	-0.35 eV	-0.46 eV	-0.40 eV
Co_3O_4	-2.66 eV	-1.53 eV	-1.82 eV	-1.13 eV
CuO	-1.08 eV	0.51 eV	-0.81 eV	-1.59 eV

3 References:

1. G. Kresse and J. Furthmüller, *Physical Review B*, 1996, **54**, 11169-11186.
2. P. E. Blöchl, *Physical Review B*, 1994, **50**, 17953-17979.
3. G. Kresse and D. Joubert, *Physical Review B*, 1999, **59**, 1758-1775.
4. J. P. Perdew, K. Burke and M. Ernzerhof, *Phys. Rev. Lett.*, 1996, **77**, 3865-3868.
5. B. Farkaš, D. Santos-Carballal, A. Cadi-Essadek and N. H. de Leeuw, *Materialia*, 2019, **7**, 100381.
6. M. Wu, J. Zhao, C. Li and R. Liu, *Journal of Materials Chemistry A*, 2022, **10**, 4791-4799.
7. H. Zhou, Y. Ren, Z. Li, M. Xu, Y. Wang, R. Ge, X. Kong, L. Zheng and H. Duan, *Nature Communications*, 2021, **12**, 4679.
8. X. Wei, Y. Li, L. Chen and J. Shi, *Angew. Chem. Int. Ed. Engl.*, 2021, **60**, 3148-3155.
9. J. Hao, J. Liu, D. Wu, M. Chen, Y. Liang, Q. Wang, L. Wang, X.-Z. Fu and J.-L. Luo, *Applied Catalysis B: Environmental*, 2021, **281**, 119510.
10. X. Han, H. Sheng, C. Yu, T. W. Walker, G. W. Huber, J. Qiu and S. Jin, *ACS Catalysis*, 2020, **10**, 6741-6752.
11. W.-J. Liu, Z. Xu, D. Zhao, X.-Q. Pan, H.-C. Li, X. Hu, Z.-Y. Fan, W.-K. Wang, G.-H. Zhao, S. Jin, G. W. Huber and H.-Q. Yu, *Nature Communications*, 2020, **11**, 265.
12. J. Li, R. Wei, X. Wang, Y. Zuo, X. Han, J. Arbiol, J. Llorca, Y. Yang, A. Cabot and C. Cui, *Angew. Chem. Int. Ed. Engl.*, 2020, **59**, 20826-20830.
13. K. Xiang, D. Wu, X. Deng, M. Li, S. Chen, P. Hao, X. Guo, J.-L. Luo and X.-Z. Fu, *Adv. Funct. Mater.*, 2020, **30**, 1909610.
14. Y. Li, X. Wei, L. Chen, J. Shi and M. He, *Nature Communications*, 2019, **10**, 5335.
15. X. Wei, S. Wang, Z. Hua, L. Chen and J. Shi, *ACS Applied Materials & Interfaces*, 2018, **10**, 25422-25428.
16. W.-J. Liu, L. Dang, Z. Xu, H.-Q. Yu, S. Jin and G. W. Huber, *ACS Catalysis*, 2018, **8**, 5533-5541.

17. N. Jiang, X. Liu, J. Dong, B. You, X. Liu and Y. Sun, *ChemNanoMat*, 2017, **3**, 491-495.
18. L. Dai, Q. Qin, X. Zhao, C. Xu, C. Hu, S. Mo, Y. O. Wang, S. Lin, Z. Tang and N. Zheng, *ACS Central Science*, 2016, **2**, 538-544.
19. B. You, X. Liu, N. Jiang and Y. Sun, *J. Am. Chem. Soc.*, 2016, **138**, 13639-13646.